Post-print of: Woloszyk K., Kahsin M., Garbatov Y.: Numerical assessment of ultimate strength of severe corroded stiffened plates.
ENGINEERING STRUCTURES. Vol. 168, (2018), p. 346-354. DOI: 10.1016/j.engstruct.2018.04.085

Numerical Assessment of Ultimate Strength of Severe Corroded Stiffened Plates

K. Woloszyk[a], M. Kahsin[a], Y. Garbatov[b, 1]

[a] *Faculty of Ocean Engineering and Ship Technology, Gdansk University of Technology, G. Narutowicza 11/12 st., 80-233 Gdansk, Poland*
[b] *Centre for Marine Technology and Ocean Engineering (CENTEC), Instituto Superior Técnico, Universidade de Lisboa, Avenida Rovisco Pais 1049-001 Lisboa, Portugal*

ABSTRACT

The objective of this work is to investigate numerically (using the non-linear FEM and the approach stipulated by the Common Structural Rules) the severe corrosion degradation effect on the ultimate strength of stiffened plates and compare the results of the already published experimental studies. Different factors governing the structural behaviour of corroded stiffened plates are investigated, such as corrosion degradation level, material properties, initial imperfections and boundary conditions. The numerically estimated ultimate strength demonstrated to be very close to those observed during the experimental test. A sensitivity analysis with respect to the most important governing parameters of the numerical estimation of the ultimate strength is also performed and several conclusions are derived. The applied calculation procedure avoids using of a non-uniform surface of the corroded plates and instead of that an equivalent thickness is applying leading to a relatively fast and practical approach to the ultimate strength assessment of corroded stiffened plates.

Keywords: Stiffened Plates, Corrosion, Compressive Load, Ultimate Strength, Finite Element Method

1. INTRODUCTION

Ultimate strength is one of the fundamental assessment criteria during the ship structural design and it is commonly used in the design of different metal structures. One of the first attempts to analyse the ship hull ultimate strength was performed by Caldwell [1] by applying the rigid plastic mechanism approach, where the yield stress of the buckled part of the material was reduced. Turner [2] introduced the Finite Element Method (FEM) and at first, it was used only for an elastic behaviour analysis of structures and later to evaluate the ultimate strength, where the elastoplastic large deflection become possible to be accounted only since the early 1970s.

The ultimate strength assessment of the ship hull structures (multi-step procedure) was also introduced into the Common Structural Rules [3, 4].

With the progress of the development of the numerical methods, the ultimate strength analysis becomes a common tool in the design accounting for different governing factors that initially were difficult to be included in the analytical approaches. Some examples are the initial imperfections [5], welding induced stresses [6], non-uniform corrosion

[1] Corresponding author e-mail: yordan.garbatov@centec.tecnico.ulisboa.pt; Telf (351) 21 841 7907

degradation [7] and damaged structures [8].

One of the most important degradation mechanism in the ageing metal structures is non-uniform corrosion degradation, which can create a local failure mechanism, affecting the load carrying capacity [9-11].

Paik et al. [12] investigated how pitting corrosion influences the plate strength and concluded that the decrease of plate ultimate strength is very significant and the smaller cross-sectional area of the plate governs the ultimate strength when the plate is subjected to an axial compressive load. Paik et al. [12] also analysed the ultimate strength behaviour of welded steel plates subjected to biaxial loading with various initial imperfection shapes. Besides the initial imperfection amplitude, the shape of the initial imperfection has a significant effect on the ultimate strength and it is influencing the in-plane stiffness.

Saad-Eldeen et al. [13] experimentally tested three corroded box girders subjected to pure vertical bending loads and analysed the initial and post-collapse plate deflections concluding that, for a certain slenderness ratio, the initial imperfection shape governs the post-collapse.

The influence of a randomly distributed corrosion thickness on the ultimate strength of rectangular steel plates was investigated in [14], using the Monte Carlo [15] simulations for generating the corroded plate thickness distribution considering different degree of degradation and it was concluded that the shape of the corrosion pits and thickness distributions have a significant effect on the ultimate strength of corroded plates. A more advanced approach for a sequence-dependent data analysis was performed based on the fast Fourier transform in [16], which allows the use of the random field approach [17] in modelling the spatial corrosion wastage of steel structures subjected to the marine environment.

Garbatov et al. [18, 19] performed tensile strength tests of small-scale severely corroded specimens identifying the mechanical properties change with a function of the degree of degradation.

The results of the experimental and numerical strength assessment of the stiffened plates subjected to severe corrosion degradation and compressive load studied in [7] are being numerically analysed in the present work, exploring the nonlinear FE method. The stiffened plate specimens, tested in this experiment, are with the different corrosion degradation levels, initial imperfection shapes and amplitudes and are about a 325-mm length and 185 mm wide and the flat-bar stiffener height is 25 mm. The small-scale test specimens were taken from steel box girders subjected to a real corrosive environment in a direct contact with open seawater [20].

2. FINITE ELEMENT MODEL

The finite element model is generated employing the commercial software ANSYS [21]. The FE analysis is using the Arc-Length Method, the so-called modified Riks method. The structural configuration, including the coordinate system and boundary conditions, is shown in Figure 1. The boundary conditions are modelled as closely as possible to the ones of the experimental test performed in [7].

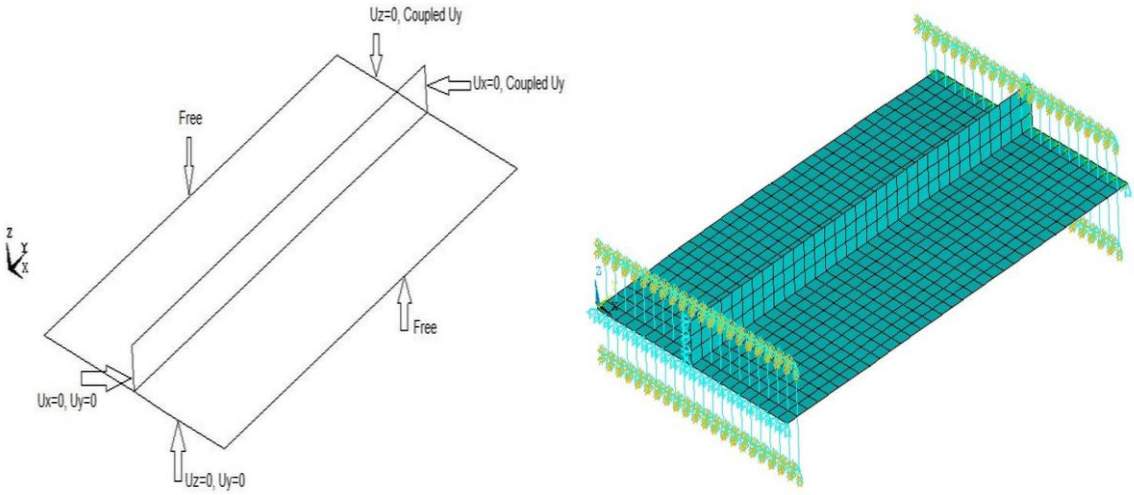

Figure 1: Geometrical FE model of stiffened plate

During the experimental test [7], the rotation of the short edges was partially constrained using clips fitted with rubber. To simulate that, spring elements COMBIN14 are used. The spring constant is linearly changing from 0 to the estimated value (based on the comparison of the edge behaviour during the experiment and in the finite element analysis) during the loading process. It is modelled in a way that, in the beginning, the edges can rotate almost freely, and as the loading is increasing, during the experimental test and numerical analysis, the degree of freedom is limited arriving at the end to the almost constrained edges. The SHELL181 finite elements are used to generate the rest of the finite element model.

To perform the non–linear ultimate strength analysis, the initial imperfections are induced by imposing the real measured amplitudes and shapes by shifting the nodal location of the finite elements without introducing any initial residual stresses. The measured initial imperfection [7] is shown in Figure 2 (left) and the generated plate surface in Figure 2 (right).

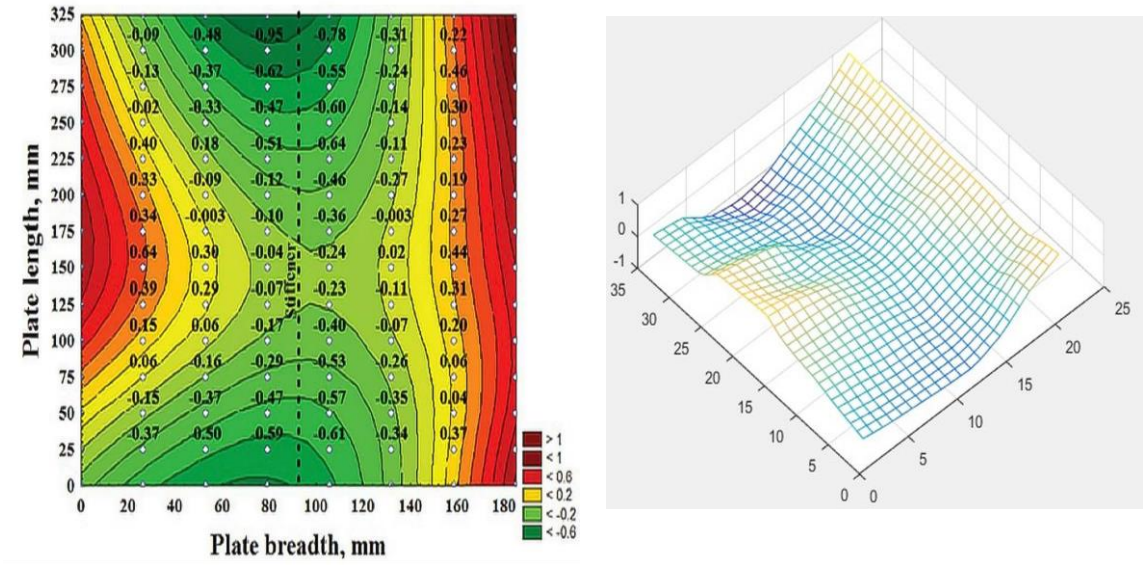

Figure 2: Measured [7] (left) and modelled (right) initial imperfection, mm

The shifting of the nodal location in the FE model is performed using a macro, specially

developed for the commercial software ANSYS, where the z-surface (z-shifting of the nodal location) of any individual nodes (x, y) is defined based on a 3-D function developed based on the regression analysis, which is shown in Figure 2 (right).

The mesh calibration is about to find the size of the finite elements and with respect to that FE analysis of intact non-corroded stiffened plates are performed applying different finite element sizes and the force-displacement relationship is compared and shown in Figure 3.

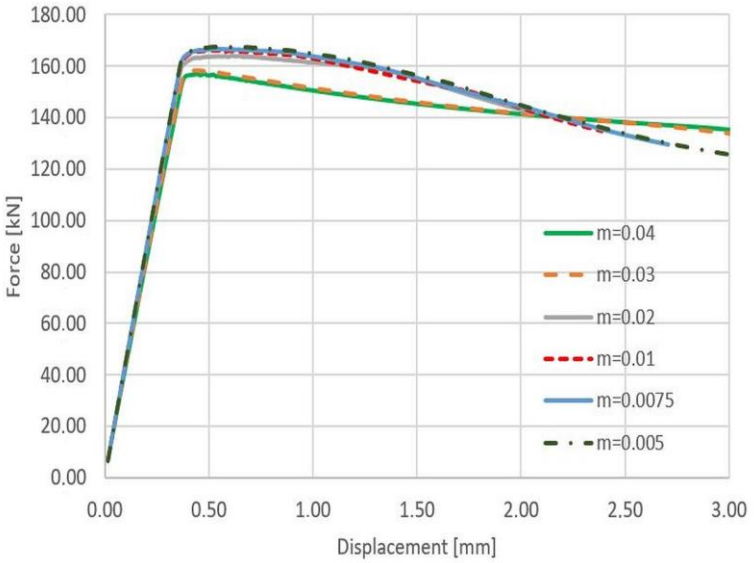

Figure 3: Mesh refinement study

Very similar results are obtained for the finite element size of 0.01 m and less and it is assumed to be used in the further FE analyses. However, a smaller element size will significantly increase the time of computations.

The corrosion degradation depth is modelled by an equivalent uniform corrosion depth, estimated based on the weight of each corroded specimen. The surface of the FE model is smooth and it is not accounting for the local corrosion degradation. The corrosion degradation is modelled by changing the shell element thickness in the FE model, which keeps the position of the neutral axis in the middle of the plate thickness leading to a two-side simultaneous corrosion wastage. The surface of the real specimen is non-uniformly corroded, which influences the structural behaviour and this effect is accounted for thought the material properties as a function of the Degree of Degradation, DoD. A different possible way is to solve this problem is to generate a random field of the stiffened plate thickness [14, 16] that may need a much smaller size of finite elements.

The material in the FE model is described as a bilinear elasto-plastic one with hardening (The strain hardening modulus is equal to 0.85 GPa). The material properties are assumed to be as a function of DoD, as defined [7]:

$$E = -1.3049\ DoD + 196 \tag{1}$$

$$Re = -0.0229\ DoD^2 + 0.5551\ DoD + 235 \tag{2}$$

and the estimated material properties for each specimen are shown in Table 1.

Table 1: Specimens properties.

	DoD [%]	t_{eqv} [mm]	E [GPa]	σ_y [MPa]
Specimen 8	11	4.005	185	238.3
Specimen 7	33	3.015	162	228.4
Specimen 6	43	2.565	151	216.5
Specimen 5	45	2.475	149	213.6
Specimen 4	46	2.43	148	212.1
Specimen 3	46	2.43	148	212.1
Specimen 2	58	1.89	136	190.2
Specimen 1	70	1.35	124	161.6

The finite element analyses are performed through a two-stage procedure. In the first stage, the ultimate compressive force is estimated considering the initial DoD and in the second one, the DoD for each corroded specimen is estimated considering the defined ultimate force from the first stage and the outputs are compared to the experimental test results.

It is also considered that the DoD follows the same time dependency and if a different corrosion environment is present, the time-dependent model will be different, but the corrosion wastage dependency, DoD will remain the same [18].

3. FINITE ELEMENT ANALYSIS

3.1. Ultimate compressive force

The estimated ultimate forces of the corroded stiffened plates, considering the initial DoD and the material properties of the corroded specimens as defined in [7] are presented in Table 2 and Figure 4 and are fitted to linear regression equations.

Table 2: Ultimate forces for initial DoD (FEM analysis).

	DoD Weight reduction [%]	P_u Experiment [kN]	P_u FEM [kN]	t_{eqv} [mm]	E [GPa]	σ_y [MPa]
Specimen 8	11	143	162.3	4.005	185	238.3
Specimen 7	33	110	102.5	3.015	162	228.4
Specimen 6	43	68	73.5	2.565	151	216.5
Specimen 5	45	80	76.3	2.475	149	213.6
Specimen 4	46	78.6	71	2.43	148	212.1
Specimen 3	46	78	73	2.43	148	212.1
Specimen 2	58	36	36.6	1.89	136	190.2
Specimen 1	70	6	20	1.35	124	161.6

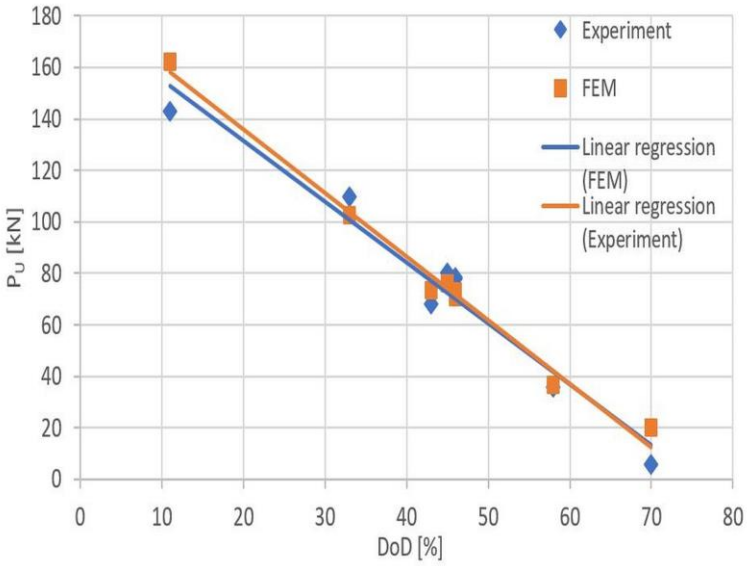

Figure 4: Ultimate compressive force as a function of DoD.

It can be seen from Figure 4 that the estimated by the FE method ultimate forces are very close to the ones that are experimentally observed. The reduction of the ultimate compressive force is due to the severe corrosion degradation effect. It should be pointed out here that the DoD, initial imperfections and material properties are not the only parameters that govern the strength reduction of the stiffened plate when corrosion degradation is present. The corrosion plate surface roughness [14] and residual stresses [6, 22, 23] can also significantly influence the reduction of the ultimate strength.

The scatter in the results can also be caused by the irregular corrosion degradation distribution on the surface of the corroded stiffened plates or due the scatter in the tensile tested corroded specimens as reported in [7]. It can be noticed that on the surface of the corroded plate specimens 1, 4 and 6 there are areas with a higher corrosion degradation depth than the average one. Ok et al. [24] showed that the plates with same DoD, but with the different pit distributions can introduce a significant variation in the ultimate strength estimation.

The reduction of the ultimate strength is also compared with the empirical formula that was developed in [25]:

$$\sigma_U/\sigma_{U0}=[(A_0-A_r)/A_0]^{0.73} \quad (3)$$

where σ_U and σ_{U0} are the ultimate strength of a structural component with and without corrosion degradation respectively, A_0 is the original cross-sectional area, A_r is the smallest cross-sectional area when the plate is subjected to corrosion degradation. The ultimate strength estimated based on the FE method and using Eqn 3, for different DoD, are presented in Figure 5.

It can be seen from Figure 5 that an agreement between Eqn 3 and the numerically and experimentally estimated ultimate strength exists, where the last one accounts for the material properties dependency of DoD of the corroded structural components. Without considering the material properties as a function of DoD of the corroded structural components, the estimated ultimate strength is being much higher.

A very similar reduction of the ultimate strength caused by the corrosion degradation can be observed in many publications as in [14, 26-28].

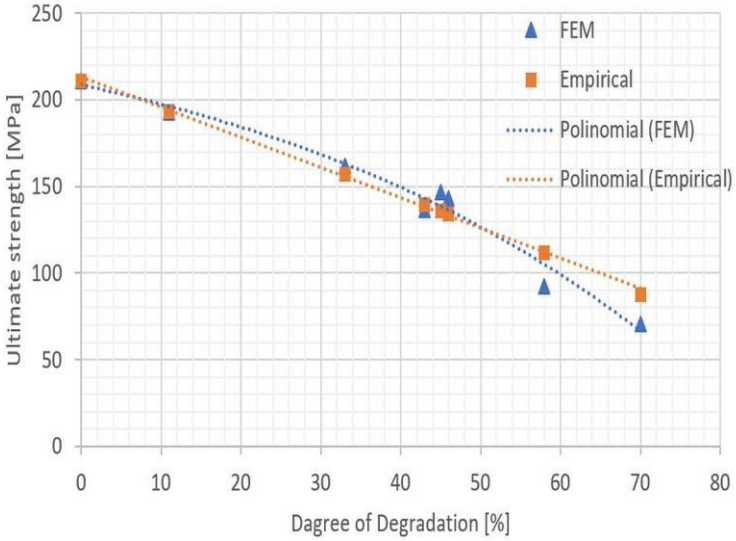

Figure 5: Ultimate strength as a function of DoD.

3.2. DoD estimate

The estimation of the force-displacement relationship here is based on the stipulated approach as given by CSR [3, 4] and it is presented in Figure 6. For each corroded stiffened plate, DoD needs to be estimated, when the ultimate force equals to the one measured during the experimental test. The results of calculations are presented in Table 3.

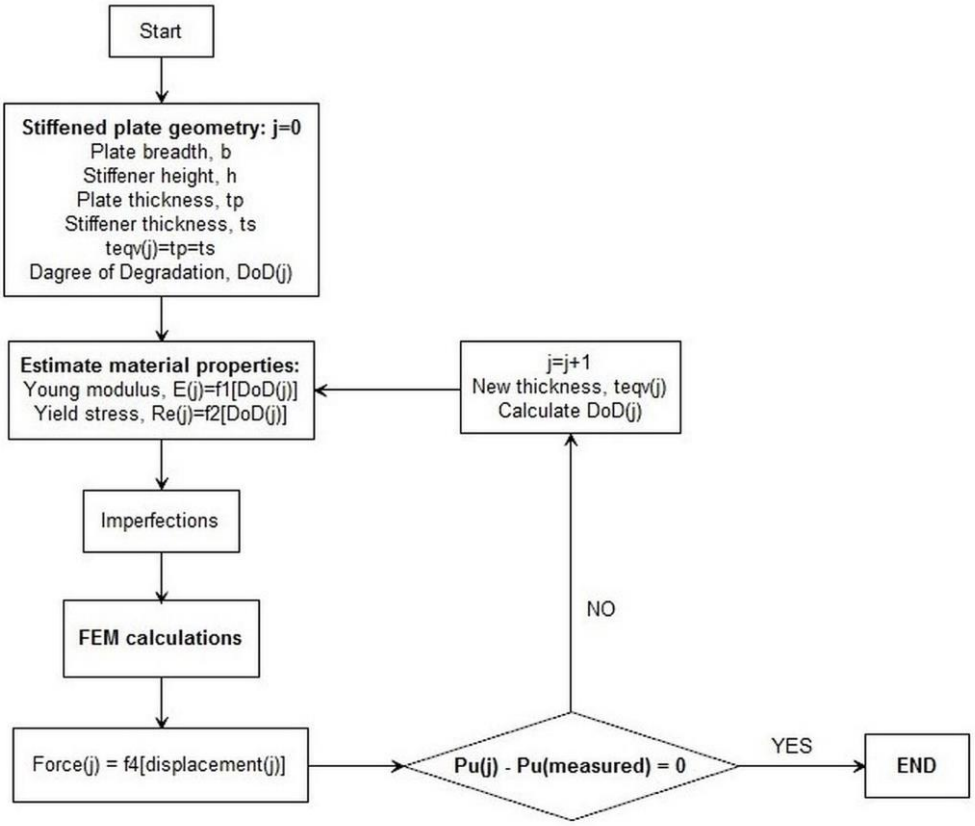

Figure 6: DoD calculation algorithm.

Table 3: Estimated DoD (FEM analysis).

	DoD (weight) [%]	P_u (measured) [kN]	t_{eqv} [mm]	DoD (FEM) [%]	E [GPa]	σ_y [MPa]	Diff (DoD) [%]
Specimen 8	11	143	3.76	16	179.0	237.9	5
Specimen 7	33	110	3.27	27	167.7	233.1	-6
Specimen 6	43	68	2.44	46	148.6	212.4	3
Specimen 5	45	80	2.68	40	154.1	220.0	-5
Specimen 4	46	78.6	2.77	38	156.2	222.5	-8
Specimen 3	46	78	2.61	42	152.5	217.9	-4
Specimen 2	58	36	1.88	58	135.7	189.7	0
Specimen 1	70	6	0.75	83	109.8	122.2	13

The DoD of the corroded stiffened plates 1, 6 and 8 is higher than the initial values, while DoD of Specimens 3, 4, 5 and 7 is lower than the initial ones. The differences can be caused also by some local effects, which are not included in the FE analysis. Figure 7 shows the estimated force-displacement relationships.

The curve shapes of the force-displacement relationships in Figure 7 are like the ones obtained in the experimental test. It can be observed that the specimens 3, 4 and 5 have similar ultimate strength, but they are having a different post–collapse behaviour. It can be

also observed that the stiffness of the pre-collapse regime of each specimen is reduced with the severity of the corrosion degradation. Similar behaviour is also observed in the experimental test [7], which is caused mostly by decreasing of the Young modulus and net–sectional area. These results also demonstrate that using the DoD dependent mechanical properties are giving good results.

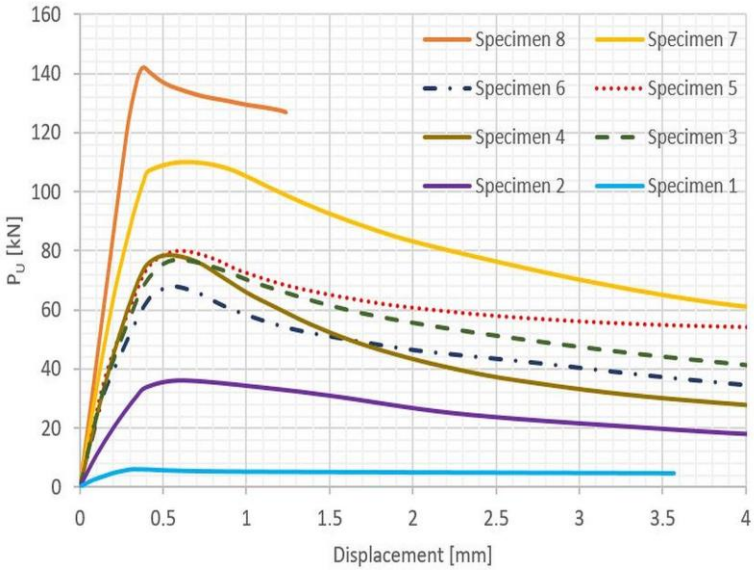

Figure 7: Force-displacement relationships, FEM

4. CSR approach

The force-displacement relationship of stiffened plates is defined based on the stipulated by CSR Rules [3, 4] approach. For each specimen, the force-displacement relationship is estimated based on the beam column buckling formulation or web local buckling of a flat bar stiffener. The results of the ultimate force for the initial DoD, which are estimated based on the weight of each corroded specimen are presented in Table 4. Figure 8 shows the ultimate forces, measured in the experiment and calculated according to the CSR stipulated approach.

Table 4: Ultimate forces for initial DoD (CSR approach).

	DoD (weight) [%]	P_u (measured) [kN]	P_u (CSR) [kN]	t_{eqv} [mm]	E [GPa]	σ_y [MPa]
Specimen 8	11	143	165.2	4.005	185	238.3
Specimen 7	33	110	75.8	3.015	162	228.4
Specimen 6	43	68	53.5	2.565	151	216.5
Specimen 5	45	80	48.5	2.475	149	213.6
Specimen 4	46	78.6	46.1	2.43	148	212.1
Specimen 3	46	78	46.1	2.43	148	212.1
Specimen 2	58	36	22.8	1.89	136	190.2
Specimen 1	70	6	8.8	1.35	124	161.6

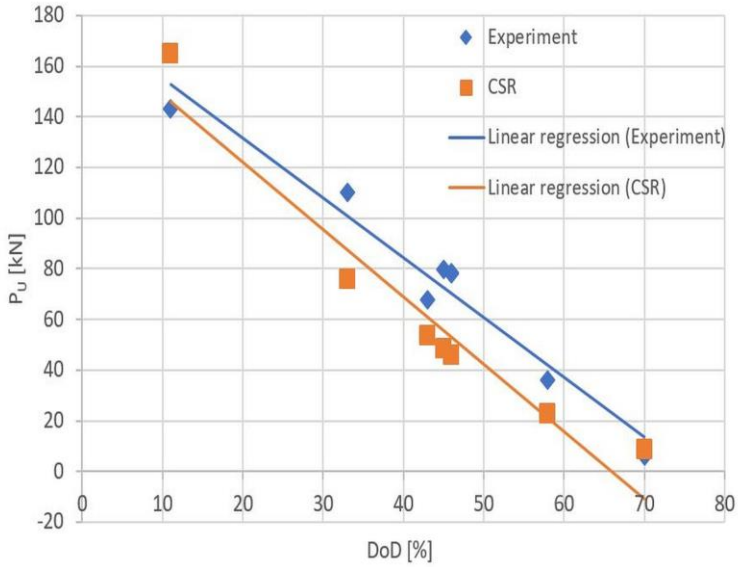

Figure 8: Ultimate force as a function of DoD.

The ultimate forces, estimated according to the CSR stipulated approach is smaller than the one measured during the experiment. The discrepancies may be caused by many reasons including the fact that the FE model cannot represent very well the boundary conditions of the experimental test and initial imperfections.

The results of the DoD calculation, when the ultimate force is equal to the one obtained in the experiment are shown in Table 5.

Table 5: Estimated DoD (CSR approach).

	DoD (weight) [%]	P_u (measured) [kN]	t_{eqv} (CSR) [mm]	DoD (CSR) [%]	E [GPa]	σ_y [MPa]	Diff (DoD) [%]
Specimen 8	11	143	3.76	17	178.9	237.9	6
Specimen 7	33	110	3.52	22	173.5	236.2	-11
Specimen 6	43	68	2.80	38	156.9	223.3	-5
Specimen 5	45	80	2.98	34	161.0	227.6	-11
Specimen 4	46	78.6	3.07	32	163.0	229.4	-14
Specimen 3	46	78	3.05	32	162.7	229.1	-14
Specimen 2	58	36	2.26	50	144.4	205.8	-8
Specimen 1	70	6	1.18	74	119.6	151..3	4

It can be noticed, that the differences in DoD are relatively higher reaching 14%. For the specimen 1 and 8, the calculated DoD is smaller than the initial one. Figure 9 shows the estimated force-displacement relationships.

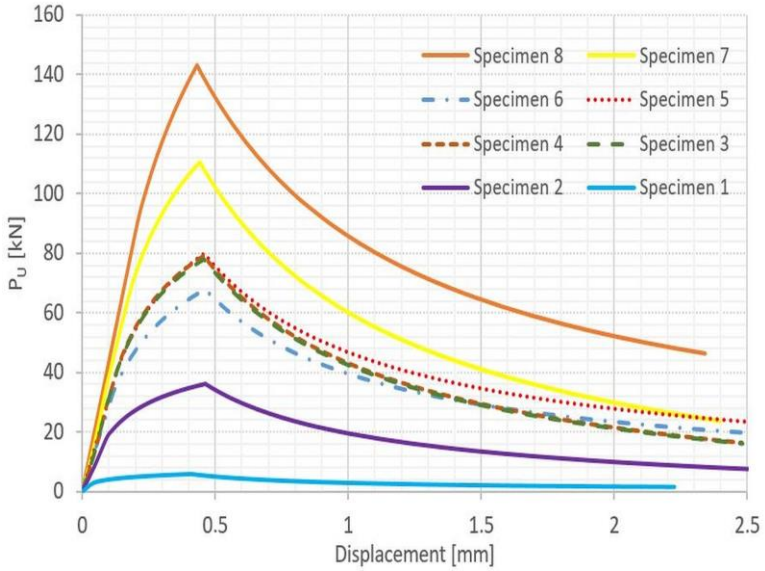

Figure 9: Force-displacement relationship, CSR Rules.

5. COMPARATIVE ANALYSIS

For each specimen, the force-displacement relationship is presented in Figure 10 to Figure 13. Generally, for all specimens, the ultimate strain estimated by FEM and CSR approach results is about 3-5 times smaller than the one recorded during the experiment test [7]. Similar observation occurs in other reported works, as for an example in [27]. Although the plate considered in this case is 8 mm thick, the phenomena observed is the same, which may be explained by the generated boundary condition in the numerical simulation and the acting forces can have some eccentricities leading to an initial bending moment.

The force-displacement relationships obtained by the FE analysis and experimental test are quite like each other in the case of the specimen 1 (Figure 10 left). The local corrosion degradation leads to a stiffener tripping and a significant loss of the ultimate strength (Fig. 14 left). This effect is not very clearly visible in the FE analysis, due to the constant thickness distribution used in the FE model (Fig. 14 right). This effect causes the big differences in the ultimate force obtained both in the case of FE analysis and CSR calculations, compared to the experimental result.

The post-collapse behaviour of the specimen 2 is similar to the experimental and FE results, whereas the curve obtained by the CSR approach has a significant drop after reaching the point of the ultimate strength (Figure 10 right). The forms of the post-collapse deformations are very like each other, as can be seen in Figure 15. It can be noticed a specific post-collapse shape of deformation, which is caused by the initial imperfection distribution.

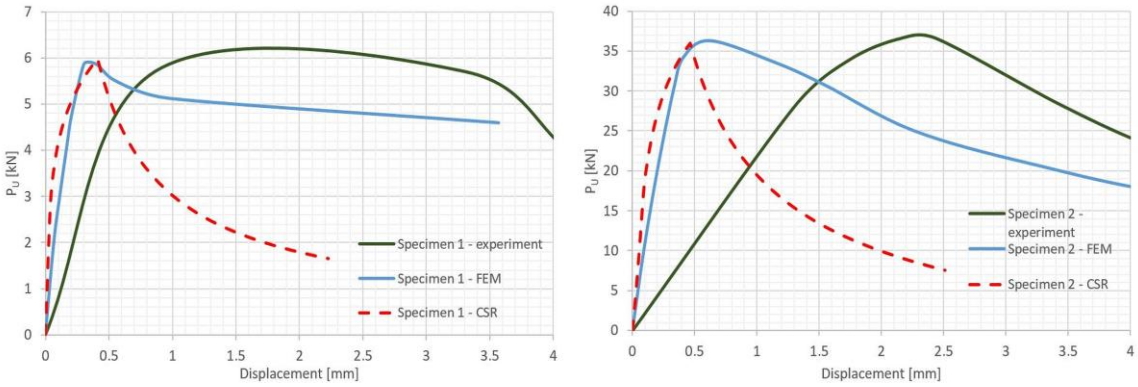

Figure 10: Force-displacement relationship of Specimen 1 (left) and 2 (right).

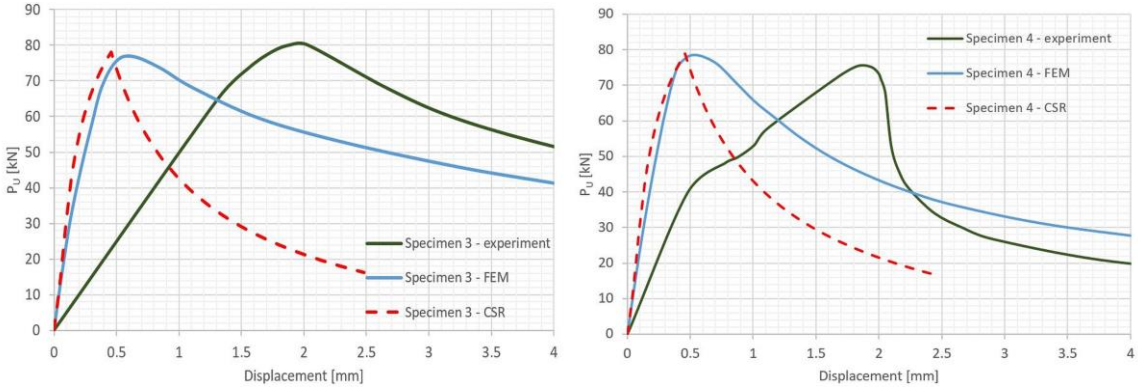

Figure 11: Force-displacement relationship of Specimen 3 (left) and 4 (right)

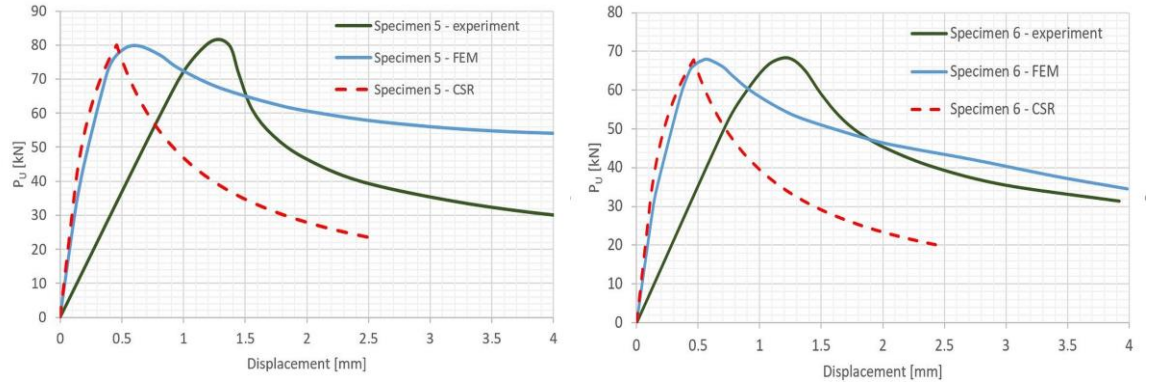

Figure 12: Force-displacement relationship of Specimen 5 (left) and 6 (right).

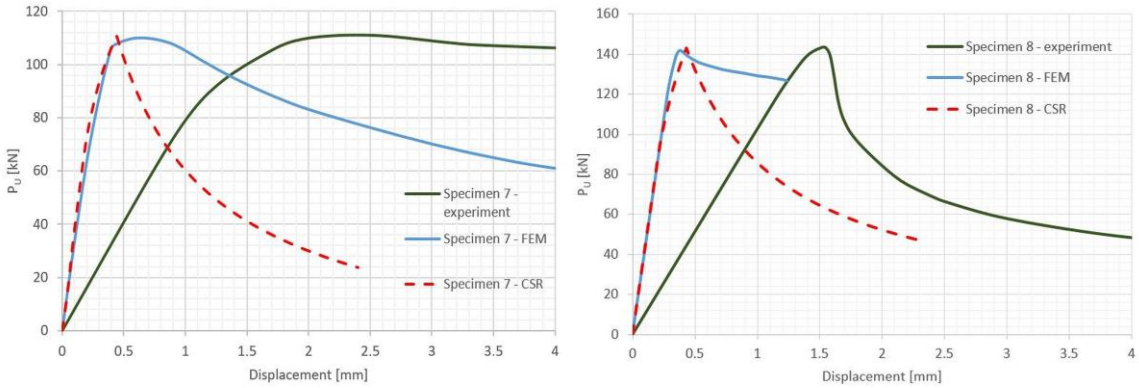

Figure 13: Force-displacement relationship of Specimen 7 (left) and 8 (right)

For the Specimen 3, the post-collapse behaviour is like the experiment and FE analysis (Figure 11 left). Comparing the post-collapse deformation as shown in Figure 16, the differences can be seen. The real specimen is dominated by global buckling, whereas the numerical model is showing local plate buckling.

Figure 11, right shows the force-displacement relationship of the specimen 4. In this case, the post-collapse behaviour is very similar (see Figure 17). The local loss of the stiffness, observed in the real corroded specimen is not observed in the FE results. It is caused by the deep corrosion degradation, which is observed in the real corroded specimen. However, the global buckling is observed both in the real corroded specimen and FE analysis, which is giving a similar post-collapse behaviour.

The post-collapse behaviour of the specimen 5 is not like the case of the FE estimate and experiment (see Figure 12, left). It can be also noticed that the CSR approach and experiment are giving similar results. The real corroded specimen has a global buckling, opposite to the FE analysis, and the specimen is dominated by the local plate buckling and the stiffener tripping (see Figure 18).

Except for the ultimate strain, the force-displacement relationship estimated by the FE analysis is very like to the one obtained in the experiment (Figure 12, right). The Specimen 6 has a global buckling towards plate buckling. The post-collapse deformation in the FE analysis is not matching exactly with the real one and the plate buckling is significant (see Figure 19).

For the specimen 7, the post-collapse regime shows the similarity between the FE analysis and experiment (Figure 13, left). In this case, the post-collapse shape of the deformation is quite like each other. In both cases, the plate buckling and stiffener tripping can be observed (see Figure 20).

For the specimen 8, the post-collapse regime in the FE analysis is not like the one obtained in experiment and CSR calculations (Figure 13, right). In the experiment, the observed form of the post-buckling collapse deformation is of the shape of the global buckling (see Figure 21), whereas in the FE analysis, the web local buckling can be observed. This can be also the reason for a higher estimated ultimate force compared to the experimental results.

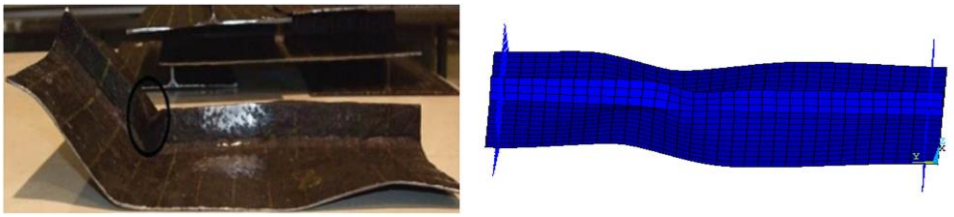

Figure 14: Tested [7] (left) and simulated (right) post-collapse shape of specimen 1.

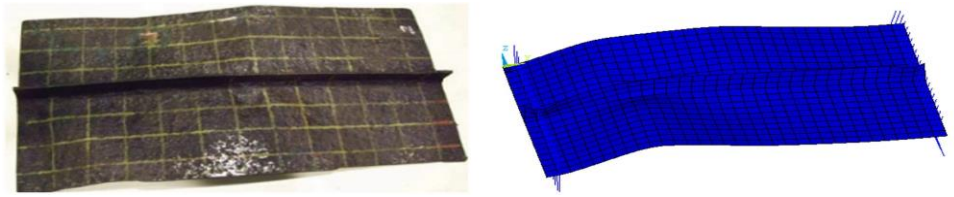

Figure 15: Tested [7] (left) and simulated (right) post-collapse shape of specimen 2

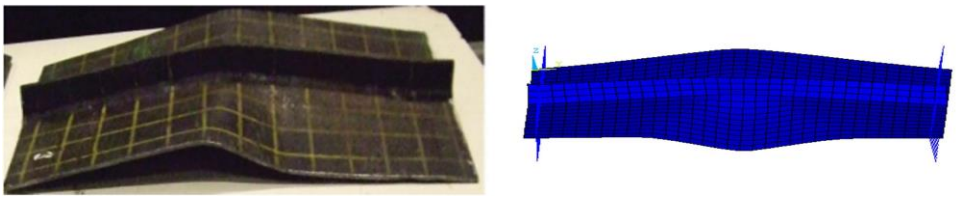

Figure 16: Tested [7] (left) and simulated (right) post-collapse shape of specimen 3.

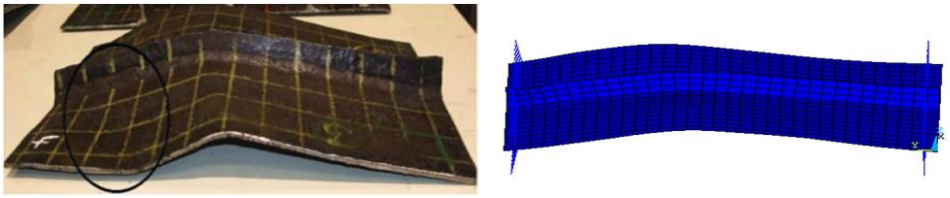

Figure 17: Tested [7] (left) and simulated (right) post-collapse shape of specimen 4.

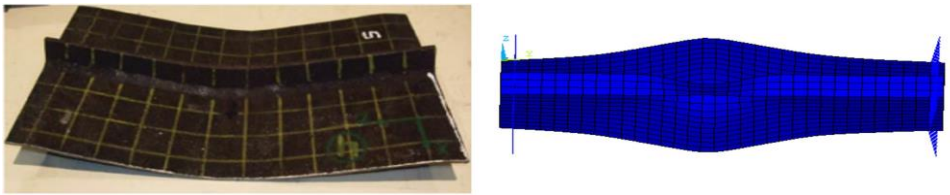

Figure 18: Tested [7] (left) and simulated (right) post-collapse shape of specimen 5.

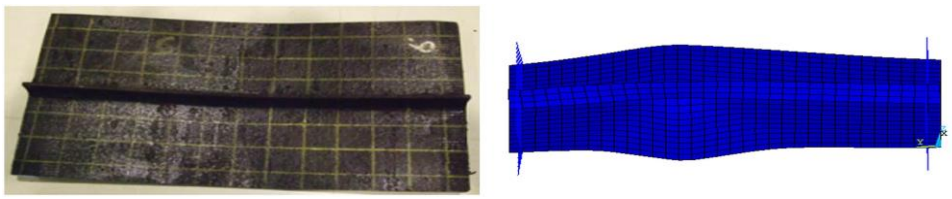

Figure 19: Tested [7] (left) and simulated (right) post-collapse shape of specimen 6.

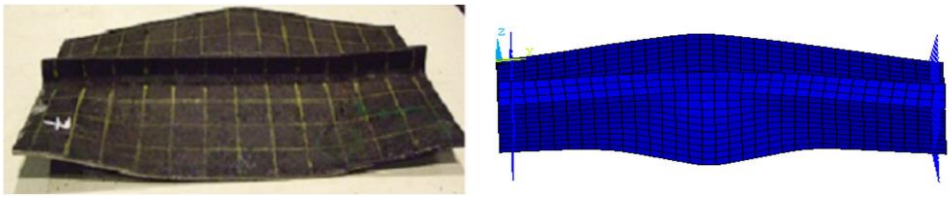

Figure 20: Tested [7] (left) and simulated (right) post-collapse shape of specimen 7.

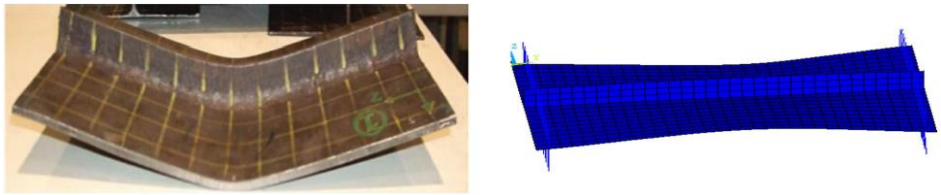

Figure 21: Tested [7] (left) and simulated (right) post-collapse shape of specimen 8.

Generally, the post-collapse shape of the deformation is matched in the experiment and FE analyses, the force-displacement relationships are also like each other. When in the tested corroded specimen, the global form of buckling is observed and local buckling is observed for FE analysis, the specimen collapses faster in the experiment.

It can be noticed, that the DoD, estimated based on the ultimate force calculated using the FE method, deviates from the one obtained by the weight measurement in the range of -8% to 13%. Also, the DoD estimated from the FE method is closer to the experimental one than the one estimated using the CSR approach. The pre-collapse regime, analysed by the CSR approach, is very like the one obtained in the FE analysis, but in the FE analysis, the ultimate strain is bigger. This can be caused due to the differences in the boundary conditions and the initial imperfection distribution.

The differences in the ultimate forces obtained in the experiment and calculated by the FE method are in the range of 10% (except the specimen 1). This can be caused by the overestimation or underestimation of the material properties, which are changing nonlinearly as a function of DoD.

The FE method is giving better results, but the CSR approach calculations are good enough to estimate the ultimate force. The CSR calculations are much simpler, which decreases the time of calculations and the needed expertise to perform the calculations.

A sensitivity analysis is also performed here in a simple way. Four governing parameters are chosen: Young modulus, yield strength, ultimate tensile stress and equivalent thickness of the corroded plate. By changing each parameter from -5 % to 5 %, the ultimate force is calculated, when other parameters are kept constant to their initial value. The initial parameter values of calculations were used for the specimen 8 model. The results of the analysis are shown in Figure 21 and Table 6.

Table 6: Sensitivity analysis results.

Parameter	-5%	-2.5%	0%	+2.5%	+5%
Young modulus [MPa]	169.8	174.2	178.7	183.2	187.6
Ultimate strength [kN]	138.3	139.7	142.0	142.8	144.2
Yield strength [GPa]	219.6	225.4	231.2	236	242.8

Ultimate strength [kN]	137.2	139.2	142.0	143.3	145.4
Ultimate stress [MPa]	380	390	400	410	420
Ultimate strength [kN]	142.0	142.0	142.0	142.0	142.0
Equivalent thickness [mm]	3.563	3.656	3.750	3.844	3.938
Ultimate strength [kN]	129.0	135.0	142.0	147.9	154.8

The variation of the impact of each governing parameter on the ultimate force is presented in Figure 21. It can be observed that the equivalent thickness, which is related to the DoD is the most significant one. When the equivalent thickness is changing from -5% to 5%, the ultimate force is changing from -9.2% to 9%. The influence of the mechanical properties is also quite significant. When the Young modulus is changing from -5% to 5%, the ultimate force is changing from -2.6% to 1.5% and when the yield strength is changed from -5% to 5%, the ultimate force is changing from -3.4% to 2.4%. Only the influence of Ultimate tensile strain is negligible, where the ultimate force is almost not changing.

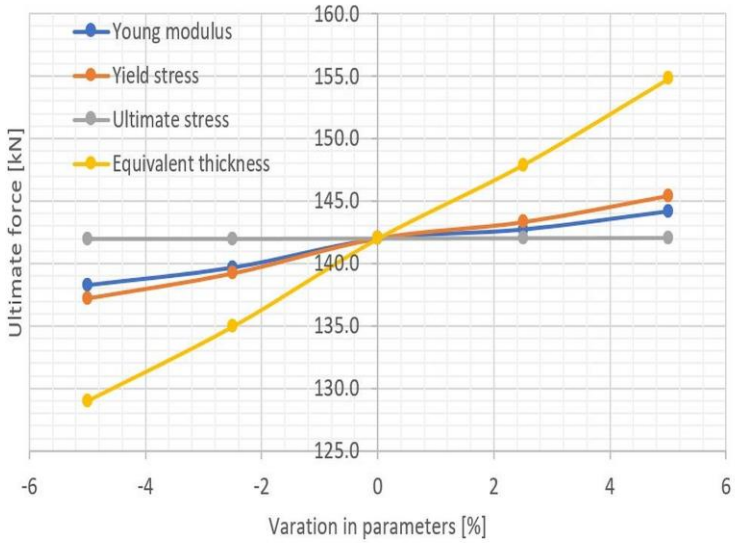

Figure 21: Ultimate force variation as a function of governing parameters.

6. CONCLUSIONS

This work presented a numerical study of the effect of the corrosion degradation on the ultimate strength of stiffened plates. The results confirmed that the corrosion degradation has a significant impact on the ultimate strength. The corrosion degradation affects not only the thickness, but also surface roughness and mechanical properties. The numerical results were compared with the experimental ones and calculations made based on the CSR approach and empirical formula, showing that the FE analyses are giving very similar results and can be used for estimating the ultimate strength of corroded plates when the changes in mechanical properties are incorporated in the numerical model. The initial structural imperfection as well as the appropriate implementation of the boundary conditions is crucial to the numerical estimates, and can severely affect the results. The used calculation procedure avoids using of a non-uniform corroded surface of the corroded plates and instead of that an equivalent thickness is applying leading to a relatively fast and practical approach. This approach can

be easily used to generate the load-shortening curves of stiffened plates subjected to severe corrosion degradation, useful in assessing the ultimate strength of structural components and integral structures. In the presented study, both numerical and experimental results are in a good agreement.

7. References

[1] Caldwell J. Ultimate Longitudinal Strength. Transactions Royal Institution of Naval Architects (RINA). 1965;107:411-30.
[2] Turner M. Stiffness and Deflection Analysis of Complex Structures. Journal of the Aeronautical Sciences. 1956;23:805-23.
[3] IACS. Common structural rules for bulk carriers. London: International Association of Classification Societies; 2006.
[4] IACS. Common Structural Rules for Oil Tankers. International Association of Classification Societies. 2006.
[5] Paik J, K., Thayamballi A, K., Lee M, J. Effect of initial deflection shape on the ultimate strength behaviour of welded steel plates under biaxial compressive loads. Journal of Ship Research. 2004;48:45-60.
[6] Tekgoz M, Garbatov Y, Guedes Soares C. Finite element modelling of the ultimate strength of stiffened plates with residual stresses. In: Guedes Soares C, Romanoff J, editors. Analysis and Design of Marine Structures. London, UK: Taylor & Francis Group; 2013. p. 309-17.
[7] Garbatov Y, Tekgoz M, Guedes Soares C. Experimental and numerical strength assessment of stiffened plates subjected to severe non-uniform corrosion degradation and compressive load. Ships and Offshore Structures. 2017;12:461-73.
[8] Tekgoz M, Garbatov Y, Guedes Soares C. Strength assessment of an intact and damaged container ship subjected to asymmetrical bending loadings Marine Structures. 2018;58:172-98.
[9] Garbatov Y, Guedes Soares C, Wang G. Nonlinear time-dependent corrosion wastage of deck plates of ballast and cargo tanks of tankers. Journal of Offshore Mechanics and Arctic Engineering-Transactions of the ASME. 2007;129:48-55.
[10] Melchers R. Development of new applied models for steel corrosion in marine applications including shipping. Ships and Offshore Structures. 2008;3:135-44.
[11] Bai Y, Kima Y, Yana H, Song X, Jiang H. Reassessment of the jacket structure due to uniform corrosion damage. Ships and Offshore Structures. 2016;11:105-12.
[12] Paik JK, Thayamballi AK, Park YI, Hwang JS. A time-dependent corrosion wastage model for seawater ballast tank structures of ships. Corrosion Science. 2004;46:471-86.
[13] Saad-Eldeen S, Garbatov Y, Guedes Soares C. Analysis of plate deflections during ultimate strength experiments of corroded box girders. Thin-Walled Structures. 2012;54:164-76.
[14] Silva JE, Garbatov Y, Guedes Soares C. Ultimate strength assessment of rectangular steel plates subjected to a random localised corrosion degradation. Engineering Structures. 2013;52:295-305.
[15] Hammersley J, Handscomb D. Monte Carlo Methods. London: Methuen; 1975.
[16] Garbatov Y, Guedes Soares C. Spatial corrosion wastage modelling of steel plates subjected to marine environments. Proceedings of the 36th International Conference on Ocean, Offshore and Arctic Engineering. Trondheim, Norway2017. p. paper OMAE2017-61751.
[17] Adler R. The Geometry of Random Fields: John Wiley and Sons, Inc.; 1981.
[18] Garbatov Y, Guedes Soares C, Parunov J, Kodvanj J. Tensile strength assessment of corroded small-scale specimens. Corrosion Science. 2014;85:296-303.
[19] Garbatov Y, Parunov J, Kodvanj J, Saad-Eldeen S, Guedes Soares C. Experimental assessment of tensile strength of corroded steel specimens subjected to sandblast and sandpaper cleaning. Marine Structures. 2016;49:18-30.
[20] Garbatov Y, Guedes Soares C. Experimental evaluation of ageing marine structures. Transactions of the Society of Naval Architects and Marine Engineers. 2015;123:89-99.
[21] ANSYS. Advanced Analysis Techniques Guide. Southpointe, 275 Technology Drive, Canonsburg, PA 15317: Ansys, Inc; 2009.
[22] Tekgoz M, Garbatov Y, Guedes Soares C. Ultimate strength assessment of a stiffened plate accounting for welding sequences. In: Chang-Sup Lee S-HV, editor. Proceedings of the 11th International Symposium

on Practical Design of Ships and other Floating Structures. Changwon City, Korea: CECO; 2013. p. 1089-95.
[23] Tekgoz M, Garbatov Y, Guedes Soares C. Ultimate strength of a plate accounting for the effect of shakedown and corrosion degradation. In: Guedes Soares C, Pena F, editors. Developments in Maritime Transportation and Exploitation of Sea Resources. London, UK: Taylor & Francis Group; 2014. p. 395-403.
[24] Ok D, Pu Y, Incecik A. Computation of ultimate strength of locally corroded unstiffened plates under uniaxial compression. Marine Structures. 2007;20:100-14.
[25] Paik JK, Lee JM, Ko MJ. Ultimate compressive strength of plate element with pit corrosion wastage. Journal of Engineering for the Maritime Environment. 2003;217:185-200.
[26] Wang Y, Wharton Y, Shenoi R. Ultimate strength analysis of aged steel-plated structures exposed to marine corrosion damage: A review. Corrosion Science. 2014;86:42-60.
[27] Kim UN, Choe IH, Paik JK. Buckling and Ultimate Strength of Perforated Plate Panels subject to Axial Compression: Experimental and Numerical Investigations with Design Formulations. Ships and Offshore Structures. 2009;4:337-61.
[28] Rahbar-Ranji A. Ultimate strength of corroded steel plates with irregular surfaces under in-plane compression. Ocean Engineering. 2012;54:261-9.